Comparison of AFM and HRTEM to determine the metal particle morphology and loading of an Au/TiO_2 catalyst

Eleni Dokou [a], Eric E. Stangland [b], Ronald P. Andres [b], W. Nicholas Delgass [b] and Mark A. Barteau [a,*]

[a] *Center for Catalytic Science and Technology, Department of Chemical Engineering, University of Delaware, Newark, DE 19716, USA*
E-mail: barteau@che.udel.edu

[b] *School of Chemical Engineering, Purdue University, West Lafayette, IN 47907, USA*

Received 8 June 2000; accepted 19 September 2000

Atomic force microscopy (AFM) has been used to study the morphology of an ultrafine gold-on-titania catalyst. By using TappingMode™ AFM (TMAFM) and SuperSharp silicon probes to minimize tip radius artifacts, we determined values for the average Au particle diameter and the gold loading in good agreement with high-resolution transmission electron microscopy (HRTEM) results. These results demonstrate the ability of AFM to characterize real supported metal catalysts with small metal particles (<5 nm) and low metal loadings, achieving resolution comparable to HRTEM, but in the ambient environment.

Keywords: supported metal catalysts, Au/TiO_2 catalyst, catalyst characterization, atomic force microscopy, high-resolution transmission electron microscopy

1. Introduction

The catalytic activity of many systems has been observed to be strongly structure sensitive. An example of such a system is ultrafine gold supported on titania. Until recently, gold has found little use in catalytic applications [1–3]. Haruta et al. [4], however have demonstrated that supporting ultrafine gold particles (with diameters smaller than 5 nm) on select metal oxides drastically changes the reactivity of gold. These systems have been shown to be very active catalysts for a number of industrially important reactions, including low-temperature CO oxidation [5,6], partial oxidation of hydrocarbons [7], epoxidation of propylene [8–10], hydrogenation of carbon oxides [11] and reduction of nitrogen oxides [12].

This dramatic change in the chemistry of the Au nanoclusters supported on metal oxides, and particularly on TiO_2, depends on the size of the metal cluster and the Au/TiO_2 interface [12,13]. Model Au/TiO_2 catalysts [14,15] and theoretical studies [16] have been employed to elucidate the structure sensitivity of this catalytic system. Studies on powder catalysts have focused on the effect of several critical parameters for the Au cluster morphology, such as the Au deposition method [10,17], the structure/chemical composition of the support [5,6,18] and the pretreatment of the catalyst [19].

In addition to spectroscopic techniques, high-resolution transmission electron microscopy [5,10,15] and scanning tunneling microscopy/spectroscopy [14,20] have been used to study the size and morphology of the metal clusters and the Au/TiO_2 interface. High-resolution transmission electron microscopy is traditionally used for catalyst characterization [21], in order to obtain estimates of the size and distribution of the metal particles on powder-supported metal catalysts. Transmission electron microscopy can provide information about the elemental composition and the electronic structure of the materials, in addition to high-resolution micrographs of the structure of the material [22], and has been extensively used to study the morphology of supported metal clusters [23]. One important limitation of electron microscopic techniques, such as SEM and TEM, is that small variations in height are difficult to resolve, and some sample treatment (e.g., coating) may be required. Scanning probe microscopy techniques can overcome these restrictions, and they have been used to study and characterize catalytic systems. Most UHV-STM studies have focused on single crystal metal or metal oxide surfaces. These studies have helped elucidate reaction mechanisms, have contributed substantially to the understanding of heterogeneous catalysis, in some cases leading directly to new ideas for catalyst design [24]. STM has also been used extensively to study more realistic model catalysts: metal clusters supported on metal oxide surfaces (single crystals of small band-gap oxides, such as TiO_2 and ZnO, or thin films in the case of larger band-gap oxide supports such as MgO and Al_2O_3) [14,20,23,25–27]. Scanning tunneling microscopy can provide high-resolution images (achieving atomic resolution for 2D or tiny 3D metal clusters [24,27]), and additional spectroscopic information on the electronic structure of the metallic particles [20,25,26], but is limited to conducting samples and planar model catalysts.

AFM is very promising for the characterization of model and real catalysts because it is not limited to conductive samples. It has been used to study model catalytic systems such as foils, films, and nanostructured surfaces. It has

* To whom correspondence should be addressed.

proven particularly valuable in studies of growth of metallic or oxide nanoparticles supported on flat oxide surfaces, including studies of model supported catalysts prepared by methods such as sputtering, evaporation, spin coating and electron beam lithography [28–32]. One problem in some of the early studies of model catalysts was the displacement of the metal particles by the AFM tip in contact mode. This problem can be solved by using non-contact or TappingMode™ AFM, which has opened the way for high-resolution imaging of particles. Different techniques have been developed to immobilize and image a variety of micron-sized minerals [33]. The resolution achieved when imaging micron or submicron-sized, three-dimensional particles is usually of the order of tens or hundreds of nanometers. Previous AFM studies of catalytic materials (pillared clays and zeolites) have achieved molecular-scale resolution, but these studies have focused on small, flat surfaces and not on imaging an entire catalyst particle [34–38].

AFM has also been used to study reaction-induced morphological changes, such as the coking of selective oxidation catalysts [39], the vapor-phase reduction of metal oxides [40], the effect of different gas atmospheres on vanadia/silica model catalysts [41], the effect of pretreatment gases on model Pd/SiO_2 thin film catalysts [29,42] and the effect of the support on model Ag/α-Al_2O_3 catalysts [43].

We have developed an AFM method [44] that allows the high-resolution imaging of submicron particles. We have used this technique to image successfully a variety of submicron powders (e.g., ceria, titania) and metal-decorated oxide particles achieving, to our knowledge, the highest resolution reported for metal clusters supported on actual metal oxide particles [44,45]. In this study we demonstrate that atomic force microscopy can be used to study the morphology of an Au/TiO_2 catalyst achieving resolution comparable to HRTEM. This level of resolution may permit one to examine the effects of different parameters on surface structure and hence on the reactivity of real supported metal catalysts.

2. Experimental

2.1. Materials

The polycrystalline anatase titania powder used in this study was obtained from Aldrich Chemical Co. It is free of significant impurities (99.9+%) and has a BET surface area of approximately 8 m^2/g. The catalysts were prepared by deposition–precipitation, using a procedure similar to that of [46]. An aqueous $HAuCl_4$ solution (Strem Chemicals, 99.9% Au) containing the anatase particles was neutralized to approximately pH 7 at room temperature with a saturated Na_2CO_3 solution (Aldrich, 99.5%). The suspensions were stirred vigorously for 3–4 h before being filtered, washed three times in 100 ml hot water (approximately 323 K). The resulting material was then calcined at 673 K for 3 h [10].

The procedure used to prepare samples suitable for single-particle AFM imaging has been described in detail previously [44]. Dilute dispersions of a TiO_2 powder (approximately 10 ppm) in purified, deionized water (Millipore Milli-Q™ system) were filtered through 0.1 μm polycarbonate membranes (Nuclepore, Corning Separation Division). After drying at 60 °C for 2 h in a vacuum oven, the membrane filters were mounted onto a microscope slide using double-sided tape, in order to facilitate imaging by AFM.

2.2. High-resolution transmission electron microscopy and atomic force microscopy

The distribution of gold particles on the titania surfaces and the average particle diameter were determined using high-resolution transmission electron microscopy (HRTEM) and atomic force microscopy (AFM).

A Jeol 2000 FX electron microscope operated at 200 keV was used to obtain TEM micrographs. A Nanoscope III multimode scanning probe microscope (Digital Instruments, Santa Barbara, CA) and a Nanoscope IIIa, Dimension 3100 scanning probe microscope (Digital Instruments, Santa Barbara, CA) were used to collect height and phase shift data simultaneously, using TappingMode™ AFM (TMAFM) [47], in air, at room temperature. Two types of single-crystal silicon, single-beam cantilever probes were used in this study: TESP silicon probes (nanoprobes, Digital Instruments, Santa Barbara, CA) with a nominal tip radius of 5–10 nm and SuperSharp silicon cantilevers (nanosensors, Wetzlar-Blankenfeld, Germany), which have a nominal tip radius of 2 nm. Both probes have a resonance frequency of approximately 300 kHz.

TMAFM is performed by oscillating the probe tip and cantilever near the cantilever's resonant frequency. The probe is brought near the sample surface such that the tip strikes the surface near the bottom of each oscillation, while it is rastered across the sample. The RMS amplitude of the oscillation is maintained at a setpoint value by a feedback system that adjusts the vertical position of the sample with a piezoelectric translator. The vertical position of the sample is monitored during the scan in order to generate a topographical image of the surface. Height detection provides the actual dimensions of surface features. The lateral forces and shearing forces that are necessarily applied to the sample in contact mode AFM [48], where the tip maintains continuous contact with the sample, are avoided through the intermittent contact of TMAFM, making this a preferable mode for imaging particles/surfaces with rough morphologies. The forces applied to the surface can be controlled by the ratio of the setpoint amplitude to the free air amplitude [49]. In this work, the amplitude setpoint voltage was adjusted to 60–75% of that of the free air amplitude, resulting in moderate force imaging.

Phase shift data can be collected simultaneously with height data. Phase shift detection measures the phase lag between the drive signal and the actual tip response signal. In phase shift detection the contrast mechanism is a convolution of topography and material/chemical properties

of the surface [50]. Phase data have enhanced resolution compared to height data because the feedback response to this electronic signal is faster than the physical movement of the piezoelectric translator in the z-direction, which is measured in order to obtain height data. Phase data are only sensitive to local stiffness differences, facilitating the resolution of nanostructures [51] and providing TMAFM with indirect sensitivity for different chemical species or morphologies. Sources of contrast in TMAFM phase images are an active research area. Due to the sensitivity of phase shift detection, the data are of very high resolution. All the images presented here are not filtered.

2.3. Image analysis

To determine the average gold particle diameter, $\langle D_{\mathrm{p}} \rangle$, from TEM micrographs, at least 50 particles were measured using Optimus version 6.1 image analysis software. The Au particle dimensions were determined by analysis of the phase and height AFM images collected simultaneously, using the software supplied by Digital Instruments. In particular, to obtain the average vertical dimension of the Au particles, section analysis can be applied to selected areas of the height images (titania particle surfaces). Section analysis provides a cross-sectional height profile of the surface along a reference line, which is drawn across the region of interest. This permits accurate estimation of the vertical dimensions of the surface features, but it is difficult to apply such analysis on rough sample surfaces. For this reason, section analysis of the height data has been used to get estimates of particle heights and aspect ratios, but high-resolution phase images were used to determine the lateral dimensions of particles. The average number of Au particles used to estimate the average Au particle diameter was approximately 40. Lateral dimensions of particles in this size range can be exaggerated by finite tip radius effects. This is discussed further in section 3.

3. Results and discussion

Figure 1 is a TappingMode$^{\mathrm{TM}}$ AFM phase image of the "fresh" anatase particles, before gold deposition and calcination. The background is the Nuclepore polycarbonate membrane. The edges of the particles can be distorted as the tip climbs or descends the steep faces of the particles. The anatase crystallite consists of several primary particles, which are typically 100–200 nm in diameter. The primary particle that is highlighted is 100 nm in diameter. The anatase primaries are aggregated in multiples to give clusters with pigmentary dimensions (approximately 0.5 μm); they therefore generally have complicated morphologies. Large facets of the crystallite surface, which are smooth on the nanometer scale, are apparent.

Figure 2(a) is a HRTEM micrograph of the calcined Au/TiO_2 catalyst; it is typical for the catalyst used in this study. The gold loading is 0.2 wt%, determined by

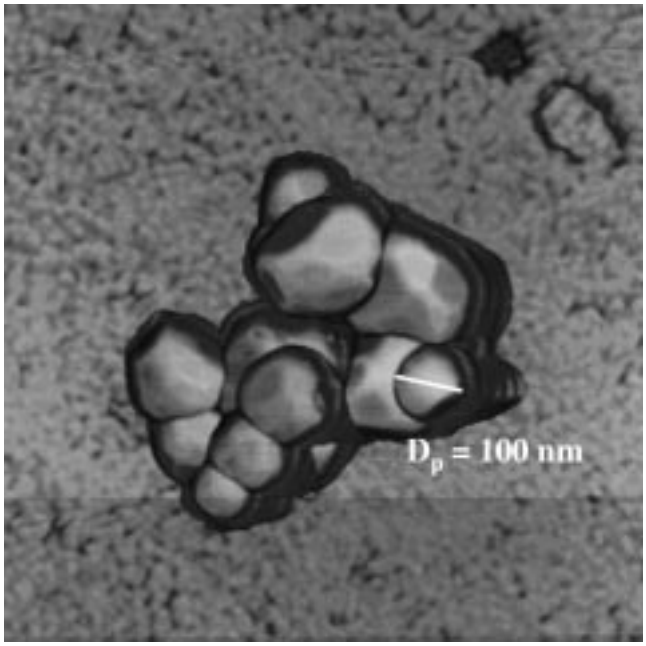

Figure 1. TappingMode$^{\mathrm{TM}}$ AFM phase image of an anatase TiO_2 particle on a Nuclepore membrane filter (scan area 1 μm $\times$ 1 μm).

atomic absorption spectroscopy (Perkin–Elmer 3110 atomic absorption spectrometer) [10]. The average gold particle diameter estimated from this particular micrograph is 3.7 ± 0.7 nm (the error bar corresponds to the standard deviation of the distribution). The average, post-calcination, Au particle size is 4.5 ± 1.0 nm, determined from a series of TEM micrographs of the catalyst [10]. Figure 2(b) is a TMAFM phase image of another catalyst particle from the same calcined sample preparation. The gold particles can be clearly imaged on the titania surfaces and their size and distribution on the TiO_2 surfaces are in good agreement with the HRTEM results. A gold particle of typical size is highlighted on the bottom right corner of the titania crystallite. It is approximately 6.9 nm in diameter. A relatively large Au particle is highlighted on the top part of the image. Its diameter is approximately 9.8 nm. The average gold particle diameter determined from this particular image is 7.88 ± 1.54 nm. This is almost two times the average size estimated by HRTEM. This difference is attributed to a tip-broadening artifact, as explained below.

AFM is not typically used to study the morphology of real catalysts with low metal loadings and small metal particle size because of the limitations to the resolution that can be achieved with TMAFM in air. The major factor that limits the resolution is the curvature of the probe. In the case of standard single-crystal Si cantilevers used for tapping mode, the nominal radius of curvature of the probe is approximately 5–10 nm. When imaging surface features with similar sizes, or even smaller than the probe itself, one produces AFM images that are a convolution of the tip shape and the sample topography [52]. In effect, structures smaller than the tip diameter will appear to be as large as the tip diameter [30,53]. The small surface features in this

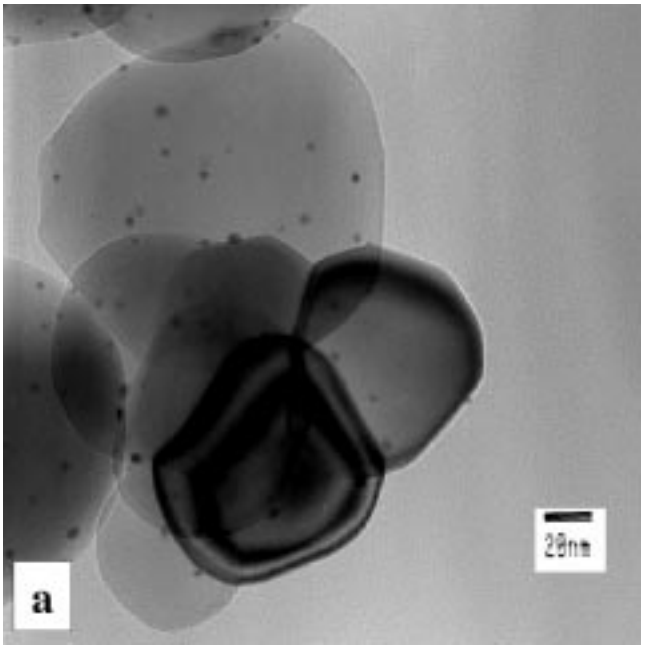

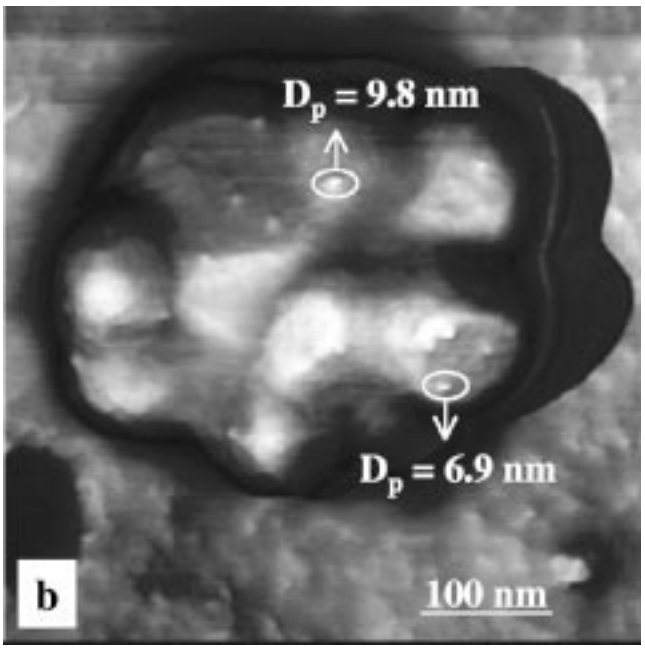

Figure 2. (a) Transmission electron micrograph of an Au/TiO_2 catalyst particle. (b) TMAFM phase image of an Au/TiO_2 catalyst particle, collected using a standard TESP silicon probe (scan area 500 nm $\times$ 500 nm).

case essentially act as tips to image the morphology of the probe. The lateral dimensions of the surface features thus are less reliable indications of particle size in this range if one does not correct for finite tip radius effects. In general, the dimensions of the probe limit the lateral resolution of the surface features. The smallest features that can be laterally resolved in phase images are in the order of a few nanometers ($<$5 nm for a SuperSharp Si probe). The resolution in the vertical direction is usually much better than the lateral resolution, and for relatively flat sample surfaces it can be of the order of a few ångstroms.

In order to estimate the dimensions of the surface features, one can use section analysis of the height images to obtain the vertical dimensions. The three-dimensional height data contain information on the actual dimensions of the surface features. Section analysis provides a cross-sectional profile of the surface along a reference line. However, if the metal particles are not hemispherical in shape the vertical dimension cannot be equated with the particle radius. Previous studies by both HRTEM and STM have shown initial 2D growth (i.e., low aspect ratios) for the Au clusters on (110) TiO_2 single crystals [54,55]. Furthermore, it is difficult to obtain accurate estimates of particle heights from section analysis of the height images because of the rough morphologies of the titania crystallites; here, however, we are successful in imaging Au particles ($<$5 nm in size) on the surfaces of titania particles which are two orders of magnitude larger.

In order to obtain accurate values of the lateral dimensions of the metal particles, one needs to decrease or to deconvolute the effect of the radius of curvature of the probe. One approach is to use other probes with smaller radii of curvature. By using a carbon nanotube probe and TMAFM in water, Andres et al. have successfully imaged small colloidal gold clusters (average diameter of 5 nm) on a flat silicon substrate [56]. In the present study, we used commercially available SuperSharp Si probes (Nanosensors), which have typical radii of curvature of 2 nm. Figure 3(a) is a TMAFM phase image of an Au/TiO_2 catalyst particle collected using a standard TESP silicon probe (scan area 600 nm $\times$ 600 nm). The background is the Nuclepore polycarbonate membrane. The catalyst particle is from the same calcined sample preparation. The TiO_2 cluster is approximately 400 nm long and 300 nm wide. The Au nanoparticles are clearly imaged as bright, elevated regions on the surfaces of the titania particle. The average Au particle diameter determined from figure 3(a) is 7.3 ± 2.9 nm, almost double the value determined from the HRTEM images. This is typical for finite tip radius effects [52]. Figure 3(b) is a TMAFM image of another Au/TiO_2 particle from the same catalyst sample supported on the Nuclepore membrane. The titania crystallite is approximately 165 nm long, 125 nm wide and 55 nm high. The bright spots on the particle surface correspond to the Au nanoparticles. This image was collected using a SuperSharp silicon probe (scan area 210 nm $\times$ 210 nm). In figure 3(b), using the sharper tips we observe an average Au particle diameter of 4.3 ± 0.9 nm, in excellent agreement with the HRTEM results, without any software correction for tip radius effects. We would like to stress that there is always a finite tip artifact. The images presented here are the highest resolution that we could achieve. The probes used had small radii of curvature and we take advantage of that in high-resolution phase imaging.

The Au loading of this catalyst can also be estimated from the AFM results. The dimensions of the titania particles were estimated using section analysis of the height data in order to calculate the volume/weight of the sup-

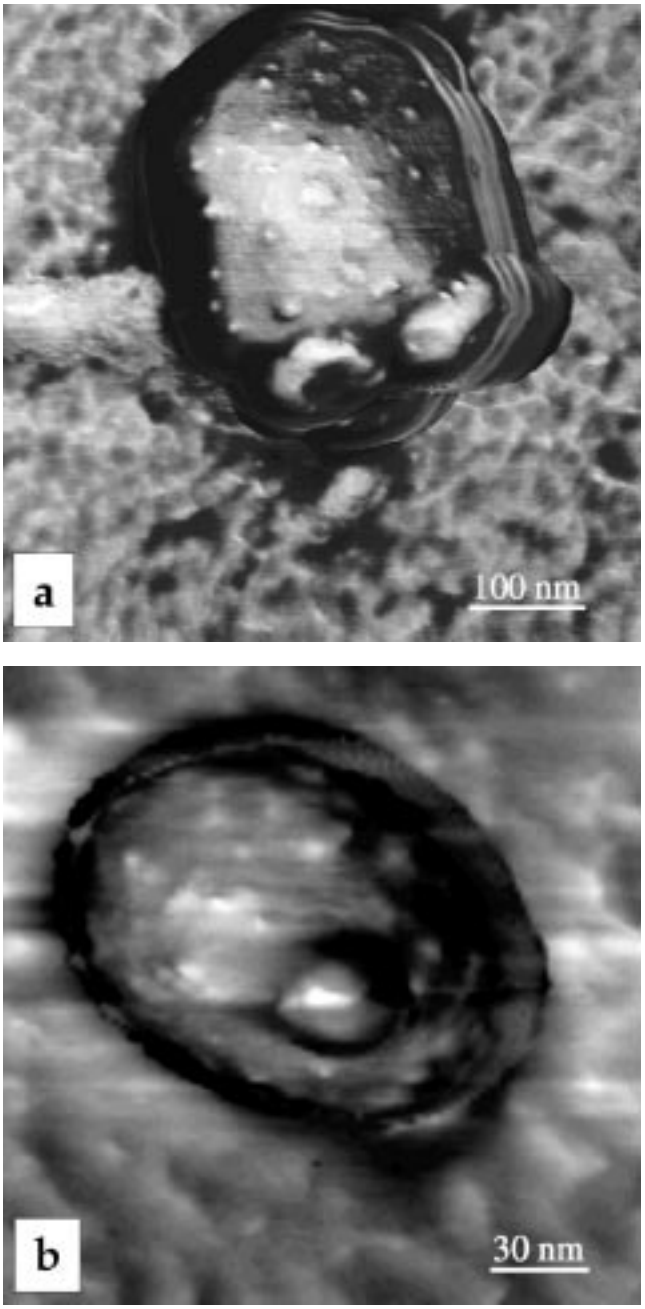

Figure 3. TMAFM phase images of the Au/TiO_2 catalyst: (a) with a standard TESP silicon probe (scan area 600 nm × 600 nm) and (b) with a SuperSharp silicon probe (scan area 210 nm × 210 nm).

port. To estimate the volume of the Au, hemispherical gold particles were assumed and the size of the particles was calculated using the phase data lateral dimensions. Even though the Au particles are not perfectly hemispherical, we used this assumption because it is difficult to obtain more accurate estimates of particle shapes from section analysis of the height images due to the rough morphologies of the titania crystallites. The aspect ratios for the Au particles obtained from section analysis of select areas of the height images were not sufficiently small to invalidate this assumption. At very low coverages it has been reported that gold particles on TiO_2(110) are relatively flat (1–2 layers high), but with the addition of more gold the particles follow the Volmer–Weber growth mode, leading to hemispherical three-dimensional Au clusters [57]. The average Au loading calculated from the AFM data was 0.22 wt%, in good agreement with the actual 0.2 wt% that was used in the catalyst preparation, as determined by atomic absorption spectroscopy. The results for the average Au particle diameter and Au loading, summarized in table 1, show reasonable agreement between the values obtained by the two techniques. These results are somewhat qualitative because only a few characteristic images have been used to obtain the values of the gold loading. As can be seen from the images, there are differences in the Au loading for different titania particles (values measured for individual particles range from 0.15 to 0.3 wt%), thus averages over a large number of particles would be needed to improve precision.

Table 1
Results for the average gold particle diameter and the gold loading estimated using the HRTEM and AFM data.

	Average Au particle diameter (nm)	Au loading (wt%)
HRTEM	4.5 ± 1.0[a]	0.2[b]
AFM (standard TESP probe)	7.6 ± 2.2	0.14
AFM (SuperSharp Si probe)	4.3 ± 0.9	0.29

[a] The error bars correspond to the standard deviation of the distribution.
[b] This value was determined by atomic absorption spectroscopy [10].

Our results demonstrate the ability of AFM to study the morphology of supported metal catalysts with small metal particles (<5 nm) and low metal loadings (<1 wt%). To our knowledge, this is the first time that atomic force microscopy has been used to characterize real catalysts achieving resolution comparable to that of high-resolution transmission electron microscopy. The resolution is limited by the probe, but the development of sharper probes (for example, the use of single-wall carbon nanotubes) can decrease the probe diameter to 1 nm [58]. For such probe radii, finite tip effects are minimal [30]. Furthermore, AFM is performed in air and it does not require vacuum, thin specimens, or any other elaborate sample preparation techniques, all of which are typical for electron microscopy. AFM provides additional information on the morphology of the support. Three-dimensional images of the titania particles are not possible using HRTEM. Another advantage of AFM is that it is a non-destructive technique, so one can image the same area on the sample before and after surface modification [44]. This may be possible with electron microscopy as well, but exposure to the electron beam may degrade the sample surface.

In conclusion, we have used atomic force microscopy to probe the morphology of Au/TiO_2 catalyst particles. This catalyst is very active for a number of potentially important reactions, including low-temperature CO oxidation and propylene epoxidation; in both cases the performance of this system is reported to be structure sensitive. It was shown that high-resolution electron microscopy and atomic force microscopy can be used to study the morphology of

the catalysts, the dispersion and the average diameter of the Au particles. AFM can successfully probe the surface structure of metal-decorated oxide particles with very high spatial resolution [45]. TMAFM was used to image the supported metal catalysts, and in order to minimize tip radius effects we have used SuperSharp silicon cantilevers, in addition to the standard TESP silicon probes. The results obtained for the average Au particle diameter are in good agreement with the HRTEM results. Transmission electron microscopy can provide information about the elemental composition and the electronic structure of the materials, in addition to high-resolution micrographs of the structure of the material [22], and has been extensively used to study the morphology of supported metal clusters [23]. Scanning probe microscopy, and in particular atomic force microscopy, is a complementary technique, which can also provide high-resolution, three-dimensional information about the structure of real supported metal catalysts. AFM has already found some *ex situ* applications in studies of reaction-induced morphological changes of catalyst surfaces [29,38–42]. The ability to image the same particle through a series of chemical exposures [44], and designs that allow scanning probe microscopes to operate at atmospheric/high pressure and high temperature [59] are opening the way for *in situ* studies of real catalysts. The evolution of the structure and the morphology of the metal clusters can in principle be monitored during chemical reaction.

Acknowledgement

ED would like to thank Dr. William E. Farneth (DuPont Co. Experimental Station) for the use of the Nanoscope IIIa AFM, Dimension 3100.

References

[1] I.E. Wachs, Gold Bull. 16 (1983) 98.
[2] J. Schwank, Gold Bull. 16 (1983) 103.
[3] G.C. Bond and D.T. Thompson, Catal. Rev. 41 (1999) 319.
[4] M. Haruta, N. Yamada, T. Kobayashi and S. Iijima, J. Catal. 115 (1989) 301.
[5] M. Haruta, S. Tsubota, T. Kobayashi, H. Kageyma, M.J. Genet and B. Delmon, J. Catal. 144 (1993) 175.
[6] S.D. Lin, M. Bollinger and M.A. Vannice, Catal. Lett. 17 (1993) 245.
[7] T. Hayashi and M. Haruta, Shokubai (Catalysts and Catalysis) 37 (1995) 72.
[8] T. Hayashi, K. Tanaka and M. Haruta, J. Catal. 178 (1998) 566.
[9] T.A. Nijhuis, B.J. Huizinga, M. Makkee and J.A. Moulijn, Ind. Eng. Chem. Res. 38 (1999) 884.
[10] E.E. Stangland, K.B. Stavens, R.P. Andres and W.N. Delgass, J. Catal. 191 (2000) 332.
[11] A. Baiker, M. Kilo, M. Maciejewski, S. Menzi and A. Wokaun, in: *New Frontiers in Catalysis*, eds. L. Guczi et al. (Elsevier, Amsterdam, 1992) p. 1257.
[12] M. Haruta, Catal. Today 36 (1997) 153.
[13] J.-D. Grunwaldt and A. Baiker, J. Phys. Chem. B 103 (1999) 1002.
[14] M. Valden, X. Lai and D.W. Goodman, Science 281 (1998) 1647.
[15] J.-D. Grunwaldt, C. Kiener, C. Wögerbauer and A. Baiker, J. Catal. 181 (1999) 223.
[16] M. Mavrikakis, P. Stoltze and J.K. Nørskov, Catal. Lett. 64 (2000) 101.
[17] G.R. Bamwenda, S. Tsubota, T. Nakamura and M. Haruta, Catal. Lett. 44 (1997) 83.
[18] M. Okumura, S. Nakamura, S. Tsubota, T. Nakamura, M. Azuma and M. Haruta, Catal. Lett. 51 (1998) 53.
[19] Y.-S. Su, M.-Y. Lee and S.D. Lin, Catal. Lett. 57 (1999) 49.
[20] M. Valden, S. Pak, X. Lai and D.W. Goodman, Catal. Lett. 56 (1998) 7.
[21] A.K. Datye and D.J. Smith, Catal. Rev. Sci. Eng. 34 (1992) 129.
[22] J.M. Thomas and W.J. Thomas, *Principles and Practice of Heterogeneous Catalysis* (VCH, Weinheim, 1997) p. 213.
[23] C.R. Henry, Cryst. Res. Technol. 33 (1998) 1119.
[24] F. Besenbacher, I. Chorkendorff, B.S. Clausen, B. Hammer, A.M. Molenbroek, J.K. Nørskov and I. Stensgaard, Science 279 (1998) 5358.
[25] D.R. Rainer, C. Xu and D.W. Goodman, J. Mol. Catal. A 119 (1997) 307.
[26] C. Xu, W.S. Oh, G. Liu, D.Y. Kim and D.W. Goodman, J. Vac. Sci. Technol. A 15 (1997) 1261.
[27] A. Piednoir, E. Perrot, S. Granjeaud, A. Humbert, C. Chapon and C.R. Henry, Surf. Sci. 391 (1997) 19.
[28] K. Okumura, S. Hyodo, S. Noda and Y. Maruyama, J. Phys. Chem. B 102 (1998) 2350.
[29] M. Schildenberger, R. Prins and Y. Bonetti, J. Phys. Chem. B 104 (2000) 3250.
[30] A. Partridge, S.L.G. Toussaint, C.F.J. Flipse, L.J. van IJzendoorn and L.C.A. van der Oetelaar, J. Vac. Sci. Technol. B 14 (1996) 585.
[31] M.A. Brookshier, C.C. Chusuei and D.W. Goodman, Langmuir 15 (1999) 2043.
[32] A. Avoyan, G. Rupprechter, A.S. Eppler and G.A. Somorjai, Topics Catal. 10 (2000) 107.
[33] B.R. Bickmore, M.F. Hochella, D. Bosbach and L. Charlet, Clays Clay Miner. 47 (1999) 573.
[34] J.E. Macdougal, S.D. Cox, G.D. Stucky, A.L. Weisenhorn, P.K. Hansma and W.S. Wise, Zeolites 11 (1991) 429.
[35] M.L. Occelli, S.A.C. Gould, J.M. Tsai and B. Drake, J. Mol. Catal. A 100 (1995) 161.
[36] M.L. Occelli, J.A. Bertrand, S.A.C. Gould and J.M. Dominguez, Micropor. Mesopor. Mater. 34 (2000) 195.
[37] S. Yamamoto, O. Matsuoka, I. Fukada, Y. Ashida, T. Honda and N. Yamamoto, J. Catal. 159 (1996) 401.
[38] S. Yamamoto, S. Sugiyama, O. Matsuoka, T. Honda, Y. Banno and H. Nozoye, Micropor. Mesopor. Mater. 21 (1998) 1.
[39] E.M. Gaigneaux, P. Ruiz, E.E. Wolf and B. Delmon, J. Catal. 172 (1997) 247.
[40] R.L. Smith and G.S. Rohrer, J. Catal. 180 (1998) 270.
[41] C. Schild, J. Engweiler, J. Nickl, A. Baiker, M. Hund, M. Kilo and A. Wokaun, Catal. Lett. 25 (1994) 179.
[42] K.H. Lee and E.E. Wolf, Catal. Lett. 26 (1994) 297.
[43] D.P.C. Bird, C.M.C. de Castilho and R.M. Lambert, Surf. Sci. 449 (2000) L221.
[44] W.E. Farneth, R.S. McLean, J.D. Bolt, E. Dokou and M.A. Barteau, Langmuir 15 (1999) 8569.
[45] E. Dokou, W.E. Farneth and M.A. Barteau, in: *Proc. 12th Int. Congr. on Catalysis*, Stud. Surf. Sci. Catal., Vol. 130, eds. A. Corma et al. (Elsevier, Amsterdam, 2000) p. 3167.
[46] S. Tsubota, M. Haruta, T. Kobayashi, A. Ueda and Y. Nakahara, in: *Preparation of Catalysts V*, eds. G. Poncelet et al. (Elsevier, Amsterdam, 1991) p. 695.
[47] Q. Zhong, D. Inniss, K. Kjoller and V.B. Elings, Surf. Sci. Lett. 290 (1993) L688.
[48] G. Binnig, C.F. Quate and C. Gerber, Phys. Rev. Lett. 56 (1980) 930.
[49] S.N. Maganov, V.B. Elings and M.-H. Whangbo, Surf. Sci. Lett. 375 (1997) L385.

[50] R. Brandisch, G. Bar and M.-H. Whangbo, Langmuir 13 (1997) 6349.
[51] B.B. Sauer, R.S. McLean and R.R. Thomas, Polym. Int. 49 (2000) 449.
[52] T. Miwa, M. Yamaki, H. Yoshimura, S. Ebina and K. Nagayama, Langmuir 11 (1995) 1711.
[53] K.L. Westra, A.W. Mitchell and D.J. Thomson, J. Appl. Phys. 74 (1993) 3608.
[54] L. Zhang, F. Cosandey, R. Persaud and T.E. Madey, Surf. Sci. 439 (1999) 73.
[55] S.C. Parker, A.W. Grant, V.A. Brondzie and C.T. Campbell, Surf. Sci. 441 (1999) 10.
[56] K. Moloni, M.R. Buss and R.P. Andres, Ultramicroscopy 80 (1999) 237.
[57] X. Lai, T.P.St. Clair, M. Valden and D.W. Goodman, Prog. Surf. Sci. 59 (1998) 25.
[58] H. Dai, J.H. Hafner, A.G. Rinzler, D.T. Colbert and R.E. Smalley, Nature 384 (1996) 147.
[59] J.A. Jensen, K.B. Rider, Y. Chen, M. Salmeron and G.A. Somorjai, J. Vac. Sci. Technol. B 17 (1999) 1080.